Accuracy of one-dimensional design procedures for finned-tube heat exchangers

G. Comini, S. Savino

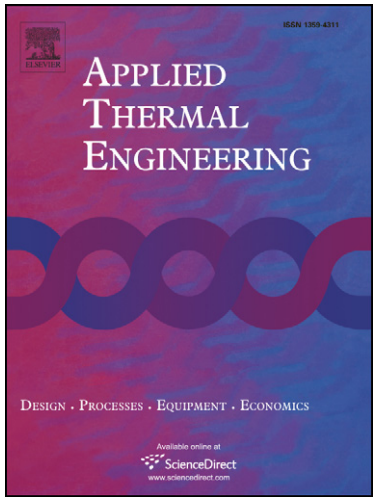

Accuracy of one-dimensional design procedures for finned-tube heat exchangers

G. Comini, S. Savino

PII: S1359-4311(09)00054-4
DOI: 10.1016/j.applthermaleng.2009.02.007
Reference: ATE 2736

To appear in: *Applied Thermal Engineering*

Received Date: 10 September 2008
Revised Date: 27 January 2009
Accepted Date: 8 February 2009

Please cite this article as: G. Comini, S. Savino, Accuracy of one-dimensional design procedures for finned-tube heat exchangers, *Applied Thermal Engineering* (2009), doi: 10.1016/j.applthermaleng.2009.02.007

Accuracy of one-dimensional design procedures for finned-tube heat exchangers

G. Comini *, S. Savino

University of Udine, Department of Energy and Fluid Machinery, Via delle Scienze 208, 33100 Udine, Italy

Abstract

In design procedures for finned-tube heat exchangers a common simplification is assuming that the temperature distribution is one-dimensional. In this way, the heat exchanger can be schematized as a thermal circuit with three thermal resistances in series: internal convection to the tube, conduction through the tube wall, and external convection through the fin assembly. The aim of this work is to quantitatively evaluate the accuracy of one-dimensional schematizations in the context of finned-tube heat exchangers utilized in air-conditioning applications. To this purpose, first three-dimensional benchmark results are obtained employing an in-house FEM code. Afterwards, a simplified two-dimensional model is proposed and validated through a comparison with the three-dimensional results. Finally, the simplified two-dimensional model and the commercial software COMSOL Multiphysics are used to conduct a parametric study aimed at assessing the accuracy of one-dimensional schematizations. The main conclusion is that the accuracy of one-dimensional design procedures is quite acceptable for practical purposes, since it leads to errors in the estimation of heat flow rates that are always less than 2 %.

Key words: Finned-tube exchangers, Overall surface efficiency, Multidimensional effects, Fin-base temperature, Air-conditioning applications

* Corresponding author. Tel.: +39 0432 558023; fax: +39 0432 558027.
Email address: gianni.comini@uniud.it (G. Comini).

Nomenclature

A	area	m^2
Bi_e	external Biot number, $Bi_e = h_e \delta_f / k$	
c_p	specific heat at constant pressure	J/(kg K)
D	external tube diameter	m
h	convection coefficient	W/(m^2 K)
k	thermal conductivity	W/(m K)
L	length	m
$\dot{m}''$	specific mass flow rate	kg/(m^2s)
n	outward normal coordinate	m
p	pressure	Pa
P	pitch	m
q	heat flow rate	W
q''	heat flux	W/m^2
r	radius and radial coordinate	m
R	thermal resistance	K/W
Re	Reynolds number, $Re = \rho u_{inf} D / \mu$	
S	spacing	m
t	temperature	° C
T	dimensionless temperature, $T = (t - t_{inf})/(t_{fi} - t_{inf})$	
$\mathbf{v}$	velocity vector	
u, v, w	velocity components	m/s
x, y, z	Cartesian coordinates	m
δ	thickness	m
Δ	dimensionless temperature depression [Eqs. (12) and (13)]	
$\bar{\eta}$	overall surface efficiency	
μ	dynamic viscosity	kg/(s m)
ξ_x	vorticity component in the x-direction	rad/s

Ω_x	dimensionless vorticity component in the x-direction, $\Omega_x = \xi_x D/u_{inf}$	
ρ	density	kg/m^3
ϑ	time	s
$\boldsymbol{\xi}$	vorticity vector	

Subscripts

b	at the fin-base
e	external
f	fluid; fin
h	convective
H	internal b.c. of the third kind (convection)
i	internal
inf	inflow
k	conductive
l	longitudinal
m	bulk [Equation (5)]
max	maximum
n	in the normal direction
out	outflow
t	tube; transverse
T	internal b.c. of the first kind (temperature)
tot	total
u	uncovered
x	in the x-direction
τ	in the tangential direction

Superscripts

$-$	average value

1 Introduction

In air-conditioning applications, heat exchangers are often of the tube-fin type, since the addition of the fins greatly increases the heat transfer area on the air-side. However, because of the finite conduction resistance of the fins, the average temperature difference between the external surface and the air-stream (and, consequently, the associated heat flow rate) decreases. A suitable measure of the resulting performance of the fin-assembly is provided by the overall surface efficiency. The overall surface efficiency is defined as the ratio between the actual rate of heat transfer from the entire surface and the maximum rate that would exist if the fin surface, as well as the exposed portion of the outer tube, were maintained at the same base temperature [1,2].

Standard design procedures for finned-tube heat exchangers rely on the knowledge of the overall surface efficiency, as well as on the assumption of approximately one-dimensional heat transport from the internal to the external fluid. In this way, the heat exchanger can be represented in terms of a one-dimensional thermal circuit with three thermal resistances in series: internal convection to the tube, conduction through the tube wall, and external convection through the fin assembly [2,3]. Furthermore, the one-dimensional schematization implies that the temperature at the fin root is uniform and equal to the outer surface temperature of the tube. This simplification paves the way to the analytical estimation of overall surface efficiencies in many situations of technical interest [1,2,4].

Unfortunately, the fin-base temperature is different from the primary surface temperature, being lower if the fin is cooled or higher if the fin is heated.

Consequently, starting from the pioneering work of Sparrow and Hennecke [5], the effects on heat transfer of the fin-base temperature depression have been repeatedly investigated. However, because of limited computer capabilities in past numerical studies and analytical difficulties in theoretical studies, the investigations of Sparrow and Lee [6], Suryanarayana [7], Look and Kang [8,9], and Juca and Prata [10] considered only fins of rectangular profile attached to a plane wall. Moreover, the accent was on the fin-base temperature depression and, consequently, reference was usually made to relatively thick fins and to relatively large Biot numbers. In this context, persistent warnings were issued on the necessity of two-dimensional design methods. In one instance, for example, the errors in heat transfer predictions resulting from two-dimensional effects were found to be as large as 80 percent [7]. On the contrary, referring to compact heat exchangers of the plate-fin type with straight thin fins of rectangular profile, Huang and Shah [11] found out that, in most situations of practical interest, the relaxation of the one-dimensional assumption does not lower more than 4 % the overall surface efficiency. In accordance with these findings, Thomas [12] showed that the large differences between one- and two-dimensional results reported in [7] were not really due to conduction effects but to a poor approximation of the average temperature of the external wall.

With the aim of establishing the reliability of the boundary conditions of the first kind that are commonly used in numerical investigations, in a most recent study Comini and Savino [13] investigated the effect of the temperature non-uniformity at the base of a fin. The conclusion reached was that the imposition of a uniform base temperature leads to an error, evaluated in terms of heat flow rates, of the order of 1 %.

In the present study the aim is the quantitative evaluation of the accuracy

of the entirely one-dimensional approximation in the design of finned-tube heat exchangers utilized in air-conditioning applications. To this purpose, first benchmark three-dimensional results are obtained by employing an in-house FEM code whose reliability had already been demonstrated through examples of application concerning compact heat exchangers of both the plate-fin and the tube-fin type [14,15,16]. Under the customary assumptions of steady state heat transfer, constant thermal conductivity of the fins, and negligible heat transfer from the outer edges, the simulations are carried out for a typical one-row tube-fin heat exchanger in the range of Reynolds numbers: $250 \leq \mathrm{Re} \leq 1000$.

Afterwards, a simplified two-dimensional model is defined to replace the original three-dimensional domain with a two-dimensional, axial-symmetric domain representing a circular fin having the same exchange area, and subjected to suitably defined "equivalent" thermal boundary conditions. The two-dimensional axial-symmetric conduction problem is solved using the commercial software Comsol Multiphysics [17], and the procedure is validated through comparisons with the three-dimensional results.

Finally, using the two-dimensional model, a parametric study is conducted to assess the accuracy of one-dimensional schematizations in design procedures for air-conditioning applications. Starting from the geometrical parameters corresponding to the three-dimensional geometry, the fin equivalent length, the outer tube diameter, the tube thickness, the fin thickness and the fin spacing are varied in the range of interest for commercial finned-tube heat exchangers. In the parametric study, reference is made to the optimal value of the external Biot number ($\mathrm{Bi}_e = 5 \cdot 10^{-5}$, in this case), which gives the maximum heat flow through a fin of given weight [18], and to two additional

Biot numbers, one order of magnitude smaller and one order of magnitude larger than the optimal value.

2 Three-dimensional model

For an incompressible, laminar flow of air, treated as a constant property fluid, forced convection is governed by the continuity equation, the Navier-Stokes equations, and the energy equation. The continuity and the Navier-Stokes equations can be written as

$$\nabla \cdot \mathbf{v} = 0 \tag{1}$$

$$\rho \frac{\partial \mathbf{v}}{\partial \vartheta} + \rho \mathbf{v} \cdot \nabla \mathbf{v} = \mu \nabla^2 \mathbf{v} - \nabla p \tag{2}$$

In the absence of volumetric heating and of significant viscous dissipation, the energy equation can be written as

$$\rho c_p \frac{\partial t}{\partial \vartheta} + \rho c_p \mathbf{v} \cdot \nabla t = k \nabla^2 t \tag{3}$$

In the above equations $\mathbf{v}$ is the velocity vector, ϑ is the time, ρ is the density, μ is the dynamic viscosity, p is the pressure, c_p is the specific heat at constant pressure, k is the thermal conductivity, and t is the temperature.

In the numerical solution, convergence to steady state is obtained through a pseudo-stationary process. As illustrated in Figure 1 (a), the computational domain encompasses both the fluid and the solid region, even if the Navier-Stokes equations are solved only in the fluid region. The energy equation is solved in both the fluid and the solid region, assuming $\mathbf{v} = 0$ in the solid region and referring to the pertinent thermophysical properties in each region.

To complete the formulation, appropriate conditions must be imposed on all boundaries.

For the Navier-Stokes equations, we impose the usual no-slip conditions $\mathbf{v} = 0$ on solid walls. At inflow, we prescribe the inlet distributions of velocity $u = u_{inf}; v = w = 0$. At outflow we impose the conditions $\partial u/\partial n = \partial v/\partial n = \partial w/\partial n = 0$ where n is the outward normal to the boundary surface. On symmetry boundaries we impose the conditions $v_n = \partial v_\tau/\partial n = 0$ where v_n is the velocity component in the normal direction and v_τ is the velocity component in the tangential direction. In the context of the numerical solution [19,20], appropriate boundary conditions for pressure are $\partial p/\partial n = 0$ applied on the whole boundary, with the value $p = 0$ specified at least in one point of the domain to fix the pressure level.

For the energy equation, at the internal surface of the tube we use either the convection boundary condition $k\,\partial t/\partial n + h_i(t - t_{fi}) = 0$ or, to simulate a very large value of h_i, the temperature boundary condition: $t = t_{fi}$. At inflow we prescribe the inlet distribution of fluid temperature $t = t_{inf}$, while at outflow and on symmetry boundaries we impose the boundary condition of the second kind $\partial t/\partial n = 0$. It must be pointed out that the continuity of temperature between the fluid and the solid region is already ensured by the model, since the interface temperature is obtained from the equation itself. Thus, no temperature boundary condition is needed at fluid-solid interfaces.

2.1 External convection coefficient

The external convection coefficient h_e can be evaluated by post-processing the results of the numerical solution. To this purpose, the heat flow rate is evaluated as

$$q = (\rho u_{inf} A_{inf}) c_p (t_{m,out} - t_{inf}) \tag{4}$$

where A_{inf} is the free inflow area, t_{inf} is the inflow temperature, $A_{out} = A_{inf}$ is the outflow area and $t_{m,out}$ is the bulk temperature at outflow

$$t_{m,out} = \frac{\int_{A_{out}} \mathbf{v} \cdot \mathbf{n}\, t\, dA}{\int_{A_{out}} \mathbf{v} \cdot \mathbf{n}\, dA} \tag{5}$$

The log-mean temperature difference is calculated from its definition

$$\Delta t_{lm} = \frac{(t_{m,out} - t_{fi}) - (t_{inf} - t_{fi})}{\ln[(t_{m,out} - t_{fi})/(t_{inf} - t_{fi})]} \tag{6}$$

by assuming, as it is very often the case in practice, that the internal fluid changes of phase. The ratio between the heat flow rate and the log-mean temperature yields the total thermal resistance

$$R_{tot} = \frac{\Delta t_{lm}}{q} \tag{7}$$

Finally, in accordance with the one-dimensional schematization illustrated in Figure 1 (b) and the standard definition of the total thermal resistance

$$R_{tot} = R_{hi} + R_k + R_{he} = \frac{1}{2\pi r_i L h_i} + \frac{1}{2\pi L k} \ln \frac{r_b}{r_i} + \frac{1}{\bar{\eta} h_e A_{tot}} \tag{8}$$

the external convection coefficient is estimated as

$$h_e = \left[\bar{\eta} A_{tot} \left(\frac{\Delta t_{lm}}{q} - \frac{1}{2\pi r_i L h_i} - \frac{1}{2\pi L k} \ln \frac{r_b}{r_i} \right) \right]^{-1} \tag{9}$$

In the above equations L is the tube length, r_i and r_b are, respectively, the internal and the external tube radii, and $A_{tot} = A_f + A_u$ is the total exchange area, sum of fin and uncovered-tube areas.

The overall efficiency is given by the expression

$$\bar{\eta} = \frac{q}{q_{max}} \tag{10}$$

where

$$q = \int_{A_{tot}} q'' \, dA \tag{11}$$

is the actual rate of heat transfer through the total area A_{tot}, and q_{max} is the maximum possible rate obtained from Eq. (11) by setting the thermal conductivity of the solid to a very large value, and simultaneously decreasing the internal convection coefficient by a suitable amount corresponding to the thermal resistance of the tube wall.

2.2 Benchmark results

Benchmark results concerning the one-row tube-fin heat exchanger illustrated in Figure 1 (a) have been obtained employing the in-house FEM code illustrated in [14,15,16]. Geometrical parameters, chosen with reference to commercial tube-fin heat exchangers, are: outer tube diameter $D = 2r_b = 10$ mm, tube thickness $\delta_t = 0.5$ mm, fin spacing $S_f = 2$ mm, fin thickness $\delta_f =$

0.2 mm, transverse pitch $P_t = 20$ mm and longitudinal pitch $P_l = 30$ mm. Because of the existing lateral and vertical symmetries, the computational domain reduces to the yellow-shaded zone which encompasses both the solid (aluminum alloy) and the external fluid (air). The thermal conductivity of the aluminum alloy is $k = 120$ W/(m K). The values of solid density and specific heat capacity have been chosen is such a way to speed-up convergence of pseudo-stationary simulations.

The external flow is laminar and can be considered incompressible. The thermophysical properties of air are: $\rho = 1.19$ kg/m^3, $\mu = 1.81{\cdot}10^{-5}$ kg/(m s), $c_p = 1.007$ kJ/(kg K), and $k = 2.58 \cdot 10^{-2}$ W/(m K). The inlet velocities u_{inf} vary in the range from 0.385 m/s to 1.52 m/s yielding Reynolds numbers, referred to the tube diameter: $\mathrm{Re} = \rho u_{inf} D/\mu$ in the range from 250 to 1000. As already stated, two different boundary conditions are utilized at the internal surface of the tube: convective boundary conditions with a value of the convection coefficient $h_i = 1000$ W/(m^{2}K) chosen in the lowest range of practical interest, and boundary conditions of prescribed temperature $t = t_{fi}$ to simulate a very large value of h_i.

Before the final runs, the distance of grid points and the time-step were decreased until further reductions did not lead to changes in the external convection coefficient h_e smaller than 1%. The final grid consisted of 90,129 nodes and 83,676 eight-node hexahedral elements and the final time step $\Delta\vartheta$ was equal to 0.0001 s.

The velocity and temperature field are better visualized by referring to dimensionless variables. The dimensionless temperature can be conveniently defined as $T = (t - t_{inf})/(t_{fi} - t_{inf})$, while the dimensionless vorticity can be defined

as $\Omega_x = \xi_x D/u_{inf}$ with reference to the ξ_x component of the vorticity vector $\boldsymbol{\xi} = \nabla \times \mathbf{v}$.

The vorticity, for all Reynolds numbers investigated, is illustrated in Figure 2 (not to scale in the vertical direction). Two representative values (one positive and one negative) of Ω_x have been considered. A comparison of the vorticity plots clearly indicates that the intensity of the vortices increase with Re and from the inflow to the outflow boundary. As expected, the presence of the tube leads to the formation of streamwise vortices in the vicinity of the fin walls.

The streamwise vortices have a strong influence on the distributions of temperatures, which are visualized in Figures 3 and Figures 4 (not to scale in the vertical direction). In the solid region, the fin temperatures decrease with the distance from the tube and increase from inflow to outflow. In the flow region, temperatures increase significantly from inflow to outflow. In both regions, temperatures are lower in Figure 3 (with convective boundary conditions) than in Figure 4 (with boundary conditions of prescribed temperature).

The circumferentially averaged temperature distributions in the tube are visualized in Figure 5 with reference to convective boundary conditions (on the left) and to boundary conditions of prescribed temperature (on the right). Obviously no temperature depression on the internal surface of the tube $r = r_i$ can arise with boundary conditions of prescribed temperature. Conversely, the boundary conditions of prescribed temperature lead to the largest temperature depression at the fin-base $r = r_b$ (as can be inferred by the larger temperature gradients in that zone). Finally, it must be pointed out that the temperature distributions in the fins are not visualized since they become one-dimensional at a very short distance from the fin-base.

The dimensionless depressions can be conveniently expressed as

$$\Delta_i = \frac{t_i - \bar{t}_i}{\Delta t_{lm}} \tag{12}$$

at $r = r_i$, and

$$\Delta_b = \frac{t_b - \bar{t}_b}{\Delta t_{lm}} \tag{13}$$

at $r = r_b$. In the above equations, reference is made to the log-mean temperature difference Δt_{lm}, the circumferentially averaged solutions t_i and t_b, and the circumferentially and axially averaged mean temperatures $\bar{t}_i$ and $\bar{t}_b$. The differences Δ_i and Δ_b are plotted vs. the dimensionless axial coordinate z/D: in Figure 6 (a) with reference to the convective boundary condition, and in Figure 6 (b) with reference to the boundary condition of prescribed temperature. As can be seen, the temperature depressions are negligible for practical purposes being always smaller than 0.02% at $r = r_i$, and 0.8% at $r = r_b$.

External convection coefficients h_e are calculated for every simulation as described in Subsection 2.1. The resulting external Biot numbers, referred to the fin-thickness ($\mathrm{Bi_e} = h_e \delta_f / k$) are reported in Table 1 as a function of the Reynolds number for convective H and temperature T boundary conditions at the internal tube surface.

As can be seen, for both H and T boundary conditions at the internal tube surface, the external Biot number Bi_e is several orders of magnitude smaller than 1, thus justifying the one-dimensional behavior of fin temperatures [4]. It is also interesting to note that the optimum Biot number $\mathrm{Bi}_e = 5{\cdot}10^{-5}$, which gives the maximum heat flow through a fin of given weight [18], is well within the range of Reynolds number investigated.

3 Two-dimensional model

The benchmark results concerning Figure 1 (a) can be utilized to identify the two-dimensional model illustrated in Figure 1 (c). As can be seen, the three-dimensional domain, which encompasses both the fluid and the solid region, is reduced to an axial-symmetric domain, which encompasses only the solid region. The definition of the equivalent outer radius $r_e = \sqrt{P_l P_t/\pi}$ ensures that the fin portion served by each tube is the same in both models. The energy equation reduces to

$$\frac{\partial}{\partial r}\left(kr\frac{\partial t}{\partial r}\right) + r\frac{\partial}{\partial z}\left(k\frac{\partial t}{\partial z}\right) = 0 \tag{14}$$

and the previously evaluated convection coefficient h_e yields the coupling between the surface of the fin-assembly and the air, whose temperature is assumed to be equal to the constant value $t_{fe} = t_{fi} - \Delta t_{lm}$. (The steady-state version of the equation is utilized since the direct stationary COMSOL solver is the most efficient in the present case).

3.1 Validation

The computational axial-symmetric domain, yellow-shaded in Figure 1 (c), is characterized by an equivalent outer radius $r_e = 13.82$ mm. The other geometrical parameters and the thermal conductivity of the solid do not change with respect to the three-dimensional model illustrated in Subsection 2.2. Furthermore, the mapped grid of two-dimensional bilinear elements matches the corresponding three-dimensional grid.

The temperature distributions in the tube are visualized in Figure 7 with

reference to convective boundary conditions (on the left) and to boundary conditions of prescribed temperature (on the right). As can be seen, there is a very good qualitative agreement between the two-dimensional results of Figure 7 with the temperature distributions of Figure 5 obtained from the circumferentially averaged three-dimensional calculations. A more quantitative comparison is presented in Table 2 where the differences $(q_{3D} - q_{2D})/q_{3D}$, between the computed values of the heat flow rates obtained from the 3D and the 2D calculations, are reported as a function of the Reynolds number for convective H and temperature T boundary condition at the internal tube surface. As can be seen, the percent differences are always less than 2%, i.e. quite acceptable for practical purposes.

3.2 Parametric study

Using the two-dimensional model, a parametric study has been conducted to assess the accuracy of one-dimensional schematizations in design procedures for air-conditioning applications. Starting from the configuration described in Subsection 2.2, and with reference to the optimal value of the external Biot number ($\mathrm{Bi}_e = 5 \cdot 10^{-5}$), five geometrical parameters (fin equivalent radius r_e, tube outer diameter r_b, tube thickness δ_t, fin thickness δ_f and fin spacing S_f) are varied in the range of interest for commercial air-conditioning heat exchangers.

The most important quantity for design purposes is the heat flow rate exchanged by the fin assembly. Thus, in Figure 8 we consider the differences $(q_{2D} - q_{1D})/q_{2D}$ between values of the heat flow rates obtained from 2D and 1D calculations. These differences are plotted versus the dimensionless ratios

ϕ between the value of a geometrical parameter and its initial value in the configuration of Subsection 2.2 (indicated by the subscript 0). As can be seen, the differences are always less than 0.01%, both for convective [Figure 8 (a)] and temperature [Figure 8 (b)] boundary condition at the internal tube surface. Two additional values of the external Biot numbers have also been considered: $\mathrm{Bi}_e = 5 \cdot 10^{-4}$ and $\mathrm{Bi}_e = 5 \cdot 10^{-6}$. The changes in $(q_{2D} - q_{1D})/q_{2D}$ brought about by the changes in Bi_e were always less than 0.015%. Thus it can be concluded that one- and two-dimensional design procedures lead to negligible differences in the calculation of heat flow rates in the whole range of interest for finned-tube exchangers utilized in air-conditioning applications.

4 Conclusions

A simplified two-dimensional model, based on the COMSOL Multiphysics software, has been first defined to analyze finned-tube heat exchangers utilized in air-conditioning applications. The simplified model has been validated trough comparisons with three-dimensional benchmark results from an in-house FEM code. It has thus been found out that the differences $(q_{3D} - q_{2D})/q_{3D}$ between heat flow rates obtained from 3D and the 2D calculations are always less than 2%, i.e. quite acceptable for practical purposes.

Afterwards, using the simplified model, a parametric study has been conducted to assess the accuracy of one-dimensional schematizations utilized routinely in design procedures. The external Biot number has been varied in the range: $5 \cdot 10^{-6} \leq \mathrm{Bi}_e \leq 5 \cdot 10^{-4}$, while five geometrical parameters (fin equivalent radius, tube outer diameter, tube thickness, fin thickness and fin spacing) have been varied in the range from 0.25 to 2 with respect to the initial value.

It has thus been found that the differences $(q_{2D} - q_{1D})/q_{2D}$ between values of the heat flow rates obtained from 2D and 1D calculations are always less than 0.015%, i.e. negligible for practical purposes.

The conclusion is that one-dimensional schematizations can be conveniently utilized in the design of heat exchangers used in air conditioning operations. With respect to three-dimensional calculations they lead, in fact, to errors in the estimation of heat flow rates that are less than 2% in the whole range of interest for finned-tube exchangers utilized in air-conditioning applications.

References

[1] F. Incropera, D. DeWitt, Fundamentals of Heat and Mass Transfer, Chapter 3, John Wiley & Sons, New York, 1996.

[2] A. Mills, Basic Heat & Mass Transfer, Chapter 2, Prentice Hall, Upper Saddle River, New Jersey, 1999.

[3] T. Kuehn, J. Ramsey, J. Threlkeld, Thermal Environmental Engineering, Chapter 11, Prentice Hall, Upper Saddle River, New Jersey, 1998.

[4] A. Bejan, Heat Transfer, Chapter 2, John Wiley & Sons, New York, 1993.

[5] E. Sparrow, D. Hennecke, Temperature depression at the base of a fin, ASME J. Heat Transfer 92 (1970) 204–206.

[6] E. Sparrow, L. Lee, Effects of fin-base temperature depression in a multifin array, ASME J. Heat Transfer 97 (1975) 463–465.

[7] N. Suryanarayana, Two-dimensional effects on heat transfer from an array of straight fins, ASME J. Heat Transfer 99 (1977) 129–132.

[8] D. J. Look, Two-dimensional fin with non-constant root temperature, Int. J. Heat Mass Transfer 32 (1989) 977–980.

[9] D. J. Look, H. Kang, Effects of variation in root temperature, Int. J. Heat Mass Transfer 34 (1991) 1059–1065.

[10] P. Juca, A. Prata, Two-dimensional fins attached to a thick wall : Effect of non-uniform root temperature, Int. J. Heat Mass Transfer 36 (1993) 233–236.

[11] L. Huang, R. Shah, Assessment of calculation methods for efficiency of straight fins of rectangular profile, Int. J. Heat and Fluid Flow 13 (1992) 282–293.

[12] L. Thomas, Heat transfer in fin assemblies: Significance of two-dimensional effects - a reexamination of the issue, ASME J. Heat Transfer 121 (1999) 748–752.

[13] G. Comini, S. Savino, Effect of temperature non-uniformity at the base of a fin, in: 5th European Thermal-Sciences Conference, Eindhoven, The Netherlands, 18-22 May, 2008.

[14] G. Comini, C. Nonino, S. Savino, Convective heat and mass transfer under dehumidifying conditions, in: R. Bennacer (Ed.), Progress in Computational Heat and Mass Transfer, Vol. II, Editions TEC & DOC - Lavoisier, Paris, 2005, pp. 711–722, invited lecture.

[15] G. Comini, C. Nonino, S. Savino, Modeling of coupled conduction and convection in moist air cooling, Num. Heat Transfer, Part A 51 (2007) 23–37.

[16] G. Comini, C. Nonino, S. Savino, Numerical evaluation of fin performance under dehumidifying conditions, J. Heat Transfer 129 (2007) 1395–1402.

[17] C. Multiphysics, COMSOL User's Guide, Version 3.2a, COMSOL AB, Stockholm, 2005.

[18] E. Eckert, R. J. Drake, Analysis of Heat and Mass Transfer, Chapter 3, McGraw-Hill Kogakusha, Tokyo, 1972.

[19] C. Nonino, G. Comini, An equal-order velocity-pressure algorithm for incompressible thermal flows, part 1: Formulation, Num. Heat Transfer, Part B 32 (1997) 1–15.

[20] C. Nonino, A simple pressure stabilization for a simple-like equal-order fem algorithm, Num. Heat Transfer, Part B 44 (2003) 61–81.

Figure Captions

- Figure 1: Schematization of a one-row tube-fin heat exchanger (a) three-dimensional domain, (b) one-dimensional thermal circuit and (c) two-dimensional axial-symmetric domain. Computational domains are not to scale.
- Figure 2: One-row tube-fin exchanger: streamwise component of the vorticity vector at different Reynolds numbers. Red colour: positive value; blue colour: negative value.
- Figure 3: One-row tube-fin exchanger: temperature fields at different Reynolds numbers for $h_i = 1000$ W/(m^{2}K). Red colour: maximum value; blue colour: minimum value.
- Figure 4: One-row tube-fin exchanger: temperature fields at different Reynolds numbers for $t = t_{fi}$ at the internal tube wall. Red colour: maximum value; blue colour: minimum value.
- Figure 5: Three-dimensional, circumferentially averaged temperature distributions in the tube wall for for $h_i = 1000$ W/(m^{2}K) on the left and $t = t_{fi}$ at the internal tube wall on the right.
- Figure 6: Dimensionless temperature differences vs. dimensionless axial coordinate: (a) at $r = r_i$ for $h_i = 1000$ W/(m^{2}K), and (b) at $r = r_b$ for $t = t_{fi}$ at the internal tube wall.
- Figure 7: Two-dimensional temperature distributions in the tube wall for $h_i = 1000$ W/(m^{2}K) on the left and $t = t_{fi}$ at the internal tube wall on the right.
- Figure 8: Percent differences $(q_{2D} - q_{1D})/q_{2D}$ between values of heat flow rates from 2D and 1D calculations plotted against the dimensionless geometrical ratios ϕ for: (a) convective and (b) temperature boundary condition at the internal tube surface.

Table 1
External Biot numbers as a function of the Reynolds number for the one-row heat exchanger of Figure 1 (a). The subscripts denote convective H and temperature T boundary conditions at the internal tube surface.

Re	250	500	750	1000
$(\mathrm{Bi}_e)_H$	$3.6{\cdot}10^{-5}$	$4.4{\cdot}10^{-5}$	$5.1{\cdot}10^{-5}$	$5.8\cdot10^{-5}$
$(\mathrm{Bi}_e)_T$	$4.5{\cdot}10^{-5}$	$5.0{\cdot}10^{-5}$	$5.6{\cdot}10^{-5}$	$6.2\cdot10^{-5}$

Table 2
Percent differences between computed values of the heat flow rates obtained from 3D and 2D calculations as a function of the Reynolds number. The subscripts denote convective H and temperature T boundary conditions at the internal tube surface.

Re	250	500	750	1000
$[(q_{3D} - q_{2D})/q_{3D}]_H$	0.7 %	1.1 %	1.7 %	1.8 %
$[(q_{3D} - q_{2D})/q_{3D}]_T$	0.9 %	1.3 %	1.7 %	1.9 %

Figure_1

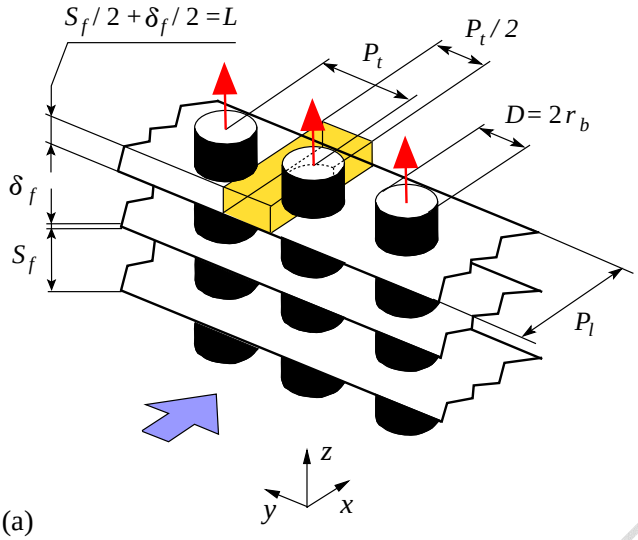

(a)

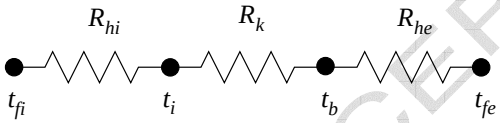

(b)

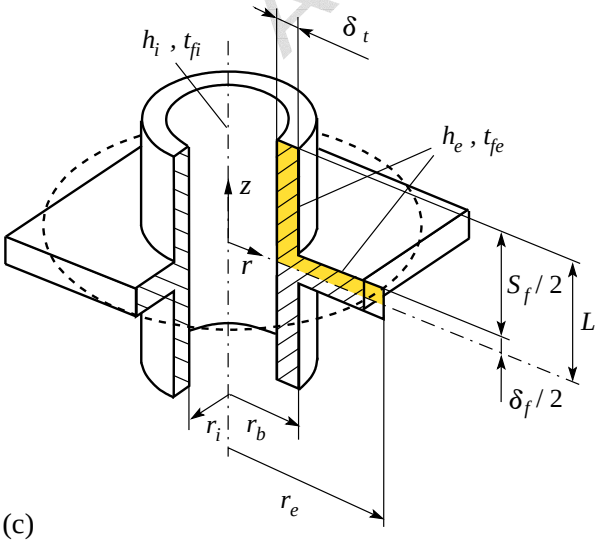

(c)

Figure_2

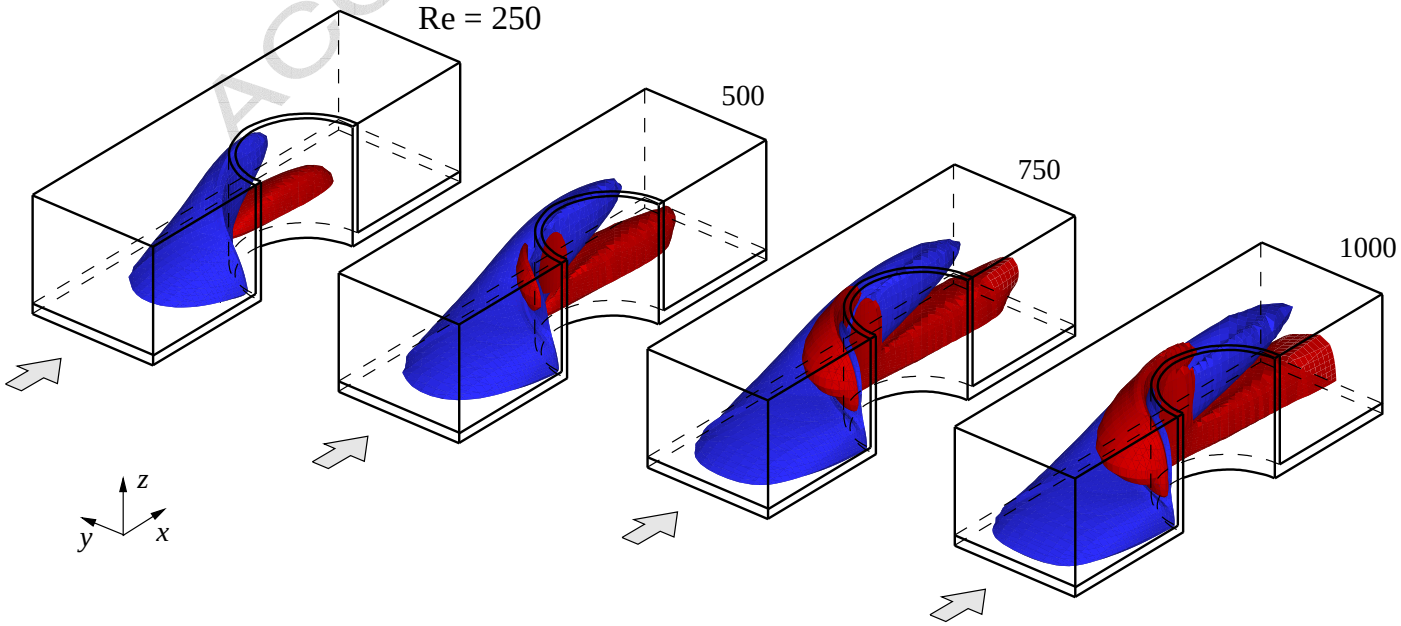

Figure_3

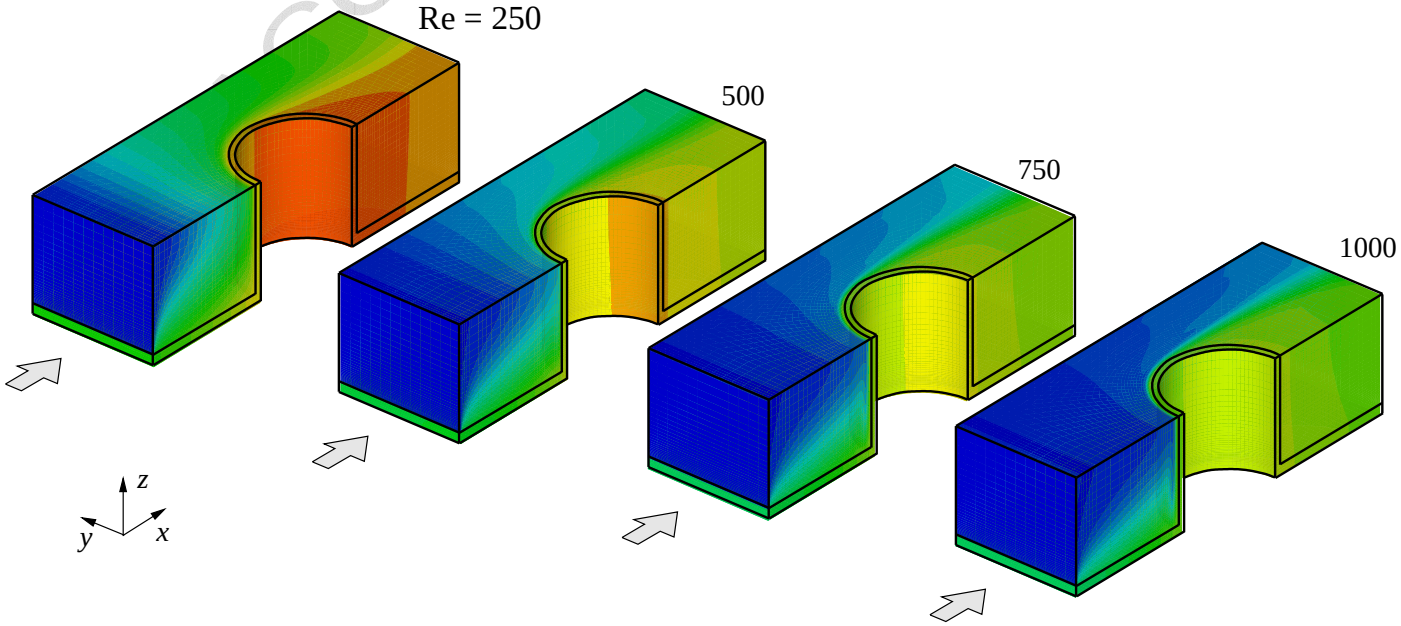

Figure_4

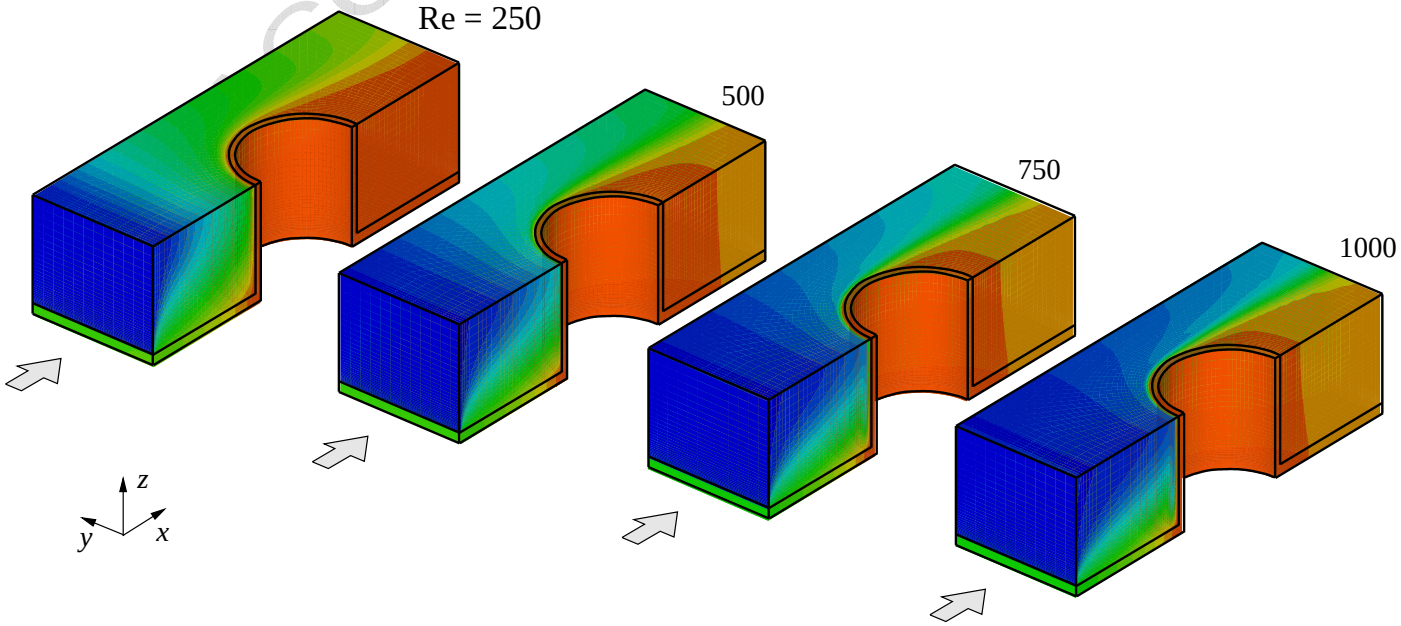

Figure_5

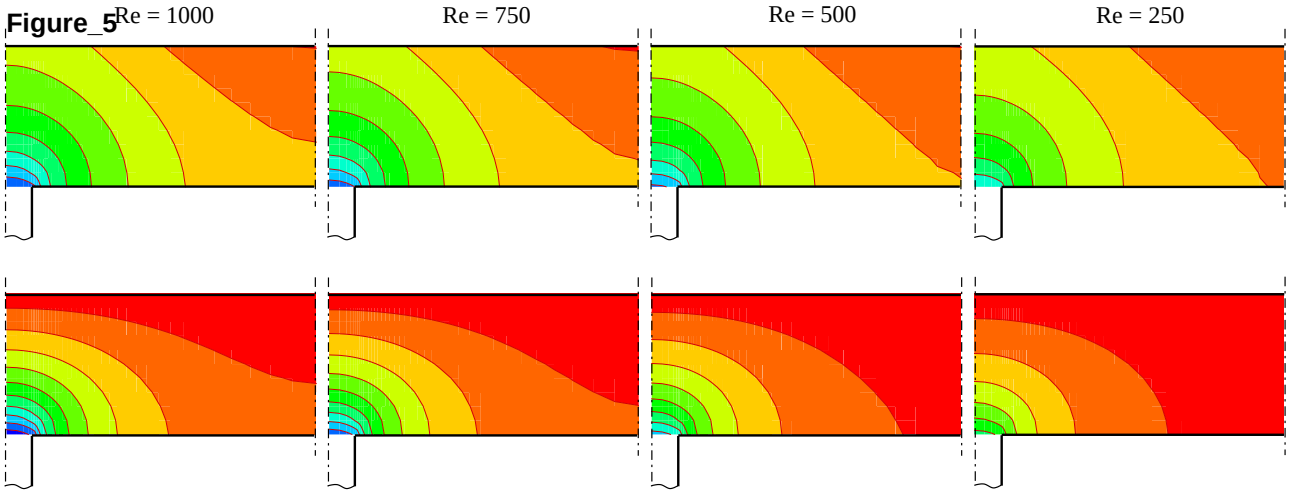

Figure_6

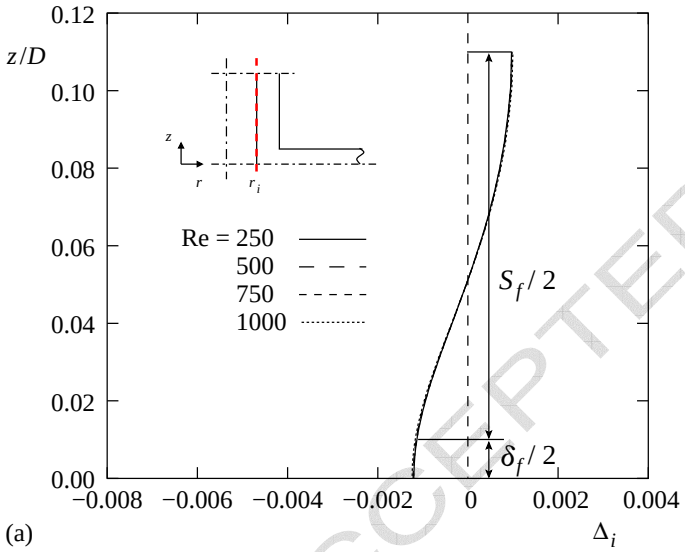

(a)

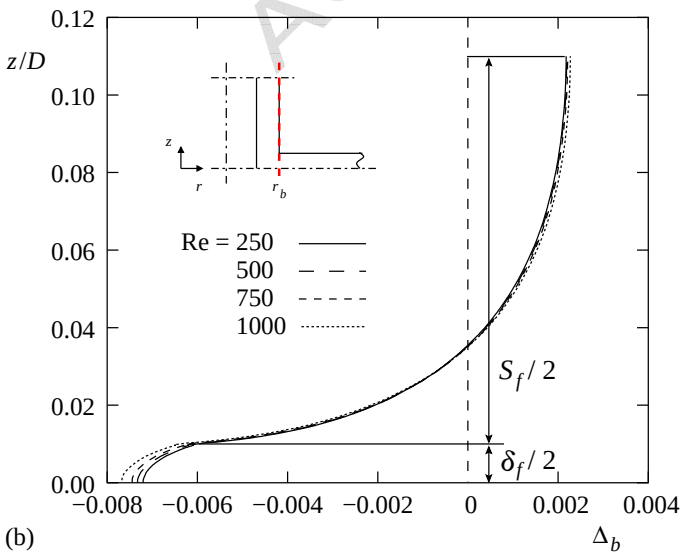

(b)

Figure_7

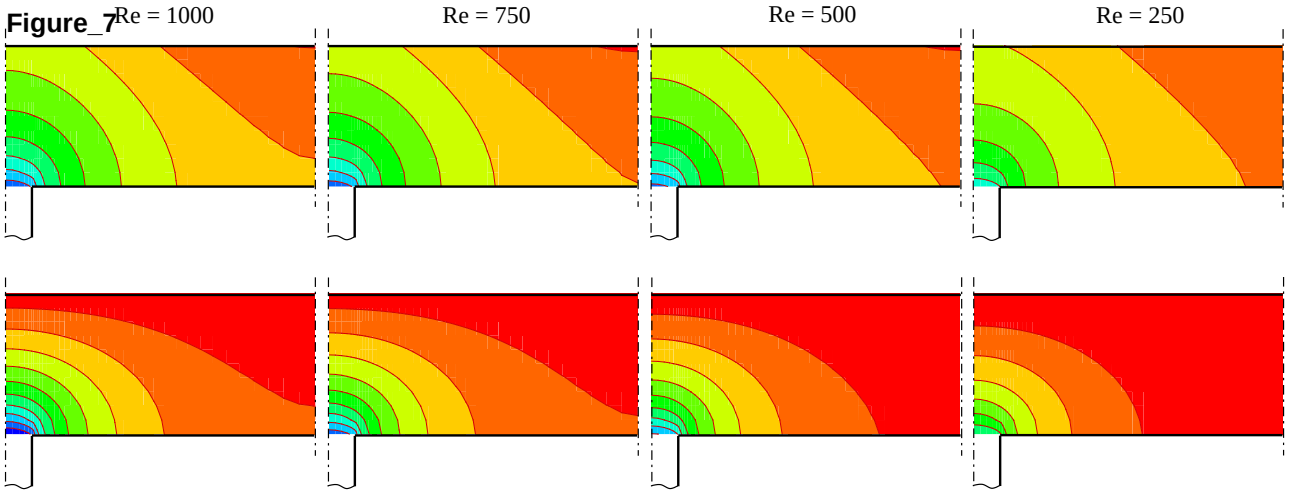

Figure_8

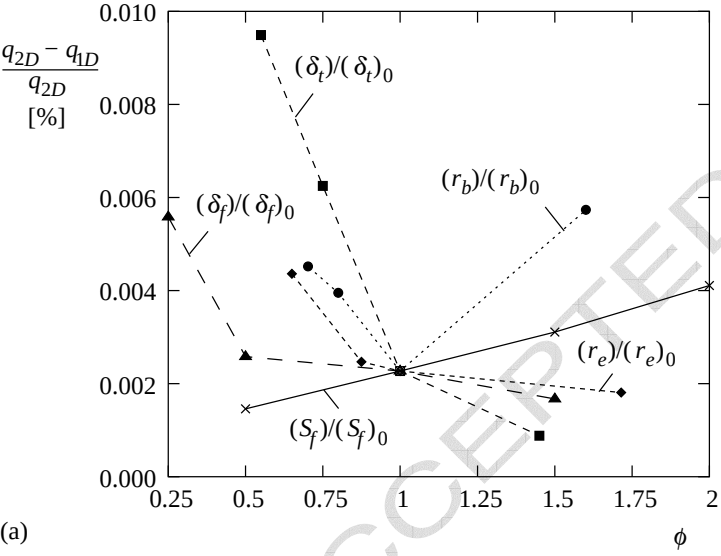

(a)

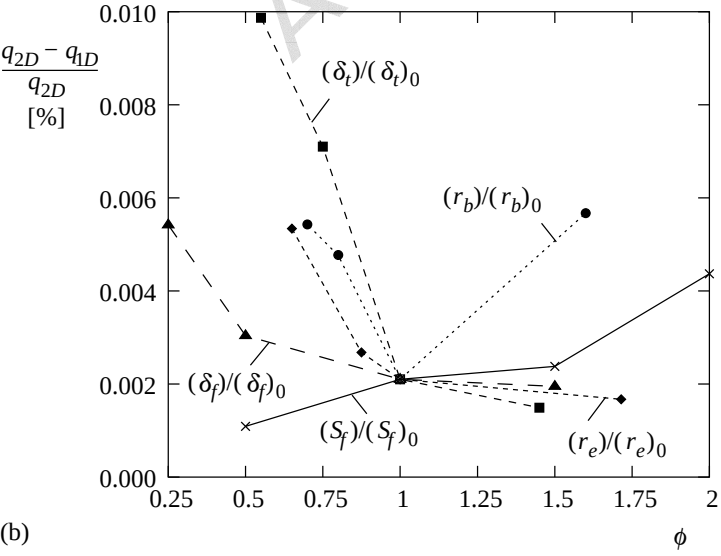

(b)